Inorganic Chemistry Communications 157 (2023) 111372

Contents lists available at ScienceDirect

Inorganic Chemistry Communications

journal homepage: www.elsevier.com/locate/inoche

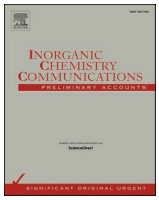

Short communication

ZnO and La-doped ZnO films by USP method and their characterizations for ultraviolet photodetectors and photocatalysis applications

Sabrina Roguai [a,b,*], Abdelkader Djelloul [a,b]

[a] LASPI²A Laboratory of Structures, Properties, and Interatomic Interactions, Abbes Laghrour University, Khenchela 40000, Algeria
[b] Science of Matter, Abbes Laghrour University, Khenchela, Algeria

ARTICLE INFO

Keywords:
ZnO films
Lanthanum
Photocatalytic properties
UV photodetectors

ABSTRACT

In this study, ZnO, Zn1-xLaxO [2, 5, 10, 15 at.%] thin films were grown on glass substrates using the spray-pyrolysis technique, to investigate the effect of doping on the structural, morphological, thermoelectric and optical properties of the layers, Also the samples were tested as UV photodetectors and photocatalyst for MB degradation. Firstly, diffraction patterns showed a hexagonal structure, with preferential grain orientation along the (002) direction, for pure ZnO and 2%La_ZnO layers, and at 5 at.% the preferential orientation changes, and crystallite sizes range from 10 nm to 19 nm. However, SEM images reveal that the ZnO and 2%La_ZnO layers are nanorods distributed over their surfaces, and the other 5%LZO, 10%LZO and 15%LZO layers characterized by nanocrystals were hexagonal prisms. The UV–visible analysis of the prepared layers shows high transparency (80–90%) in the visible range, with a constant optical gap of 3.26 eV. Thermoelectric measurements show that the ZnO and LZO layers are non-degenerate, with a maximum charge concentration of 9.18×10^{17} cm^{-3} for the 15% LZO films. The thin films show an ability for UV detection, while the 5%La_ZnO layers remain the best for UV photodetection with a good sensitivity (5.07) compared with the other layers. In terms of methyl blue degradation, the 5%La_ZnO thin films had a better degradation of 95%.

1. Introduction

Zinc oxide (ZnO) is a material with excellent properties such as a wide band gap (3.37 eV at room temperature), high exciton binding energy of 60 meV, high chemical stability, high piezoelectric constant, low dielectric constant [1]. As a result, this material can be used in gas sensors, UV light emitters, photodetectors, piezoelectric devices, solar cells and many other fields of technology [2]. The physical, optical, chemical and photocatalytic properties of ZnO can be enhanced with doping elements such as transition elements and rare earth [3]. Numerous scientific studies have focused on rare-earth-doped ZnO, with results confirming that the physico-chemical properties and transmission performance of ZnO in the visible region are enhanced by rare-earth doping. This is explained by the energy transfer between ZnO and the dopant ions, as the transition between the 4f levels make these rare earth excellent luminescence centers [4,5]. Among the rare earth, La is a good element for doping into ZnO. Thanks to their intrinsic properties of transparency and photoluminescence, transparent conducting oxides (TCOs), and ZnO in particular, are ideal as host matrices for TR ions. Lanthanum is one of the most soluble TRs, which can greatly enhance the quality of ZnO, it serves to increase oxygen vacancies [6], and consequently good polar face stability [7]. This result was recently validated by M.A. Lahmer et al [8]. Also, Sridevi et al reveal that Lanthanum doping improves the photoluminescence activity of ZnO [9]. And Xu et al.improve that the La-doped ZnO films ameliorate the optoelectronic properties, in which La in which the transmittance increase and the resistivity decrease [10].

A number of methods have been used to synthesize ZnO thin films, including RF magnetron sputtering [11], DC magnetron sputtering [12], pulsed laser deposition [13], metal organic CVD (MOCVD) [14], chemical bath deposition (CBD) [15], molecular beam epitaxy [16], spray pyrolysis [17], chemical vapor deposition [13,18], electrochemical deposition [19], sol- gel [20], screen printing [21].

In the present study, we used the ultrasonic spray pyrolysis process, a very simple, non-toxic and inexpensive method that does not require sophisticated equipment [1]. to elaborate Layers of pure and La-doped ZnO with atomic contents of 2, 5, 10 and 15% were deposited on glass substrates at 450 °C. These layers were characterized by X-ray diffraction, SEM, PL, UV–Visible spectroscopy, Seebeck coefficient, photocatalysis for methylene blue (MB) degradation and a flexible UV

* Corresponding author.
E-mail address: rog.sabrina@yahoo.fr (S. Roguai).

https://doi.org/10.1016/j.inoche.2023.111372
Received 3 June 2023; Received in revised form 17 August 2023; Accepted 4 September 2023

photodetector reacting to 365 nm light. The purpose of this study is to investigate the effect of lanthanum doping on structural, microstructural, optical, Seebeck coefficient and photoluminescence properties, and to establish a relationship between these properties and photocatalytic and UV photodetection properties.

2. Experimental part

2.1. Films preparation

To prepare $Zn_{1-x}La_xO$ layers [x = 0.00, 0.02, 0.05, 0.10, 0.15] on a cleaned glass substrate(30 × 10 × 1.2 mm^3), use a spraying solution containing zinc acetate dihydrate ($C_4H_6O_4Zn{\cdot}2H_2O$), with a molar concentration of (0.1 M), dissolved in 20 ml methanol (Merck 99.5%), 50 ml deionized water (resistivity = 18.2 MΩ cm); and 30 ml ethanol (Merck 99.5%). Lanthanum (III) acetate hydrate ($La(CH_3CO_2)_3{\cdot}xH_2O$) was added to the undoped solution during the preparation of the solution for doping such that the doping concentration in starting solution was between 2 and 15 at.%. The solutions were vigorously stirred at room temperature for 30 min until a homogeneous solution is obtained. then add a few drops of acetic acid to bring the pH to around 4.8, to inhibit hydroxide formation. For films deposition, the total volume of the solution sprayed was 50 ml and the rate of spray was 20 ml/h, 20 cm nozzle-to-substrate distance, maintained at 450 ∘C for 1 h. More detail is presented in the previous study [1,22,23].

2.2. Photodegradation of MB

The photocatalytic properties of ZnO and LZO thin films were investigated through the degradation of methylene blue solution at a concentration of 8 × 10^{-2}M, radiated by a 100 W incandescent lamp with UV light. Experiments involve emerging the photocatalyst (ZnO, ZLO) in a 250 ml beaker containing the BM solution, stirring for 30 min in the dark to achieve equilibrium adsorption–desorption of MB on the catalyst surface, and taking 10 ml of the solution and measuring its absorbance (in the dark) using a Parkin Elmer UV–VIS-NIR Lambda 19 spectrophotometer. Then, under stirring, the BM solution is irradiated with UV light and its absorbance is measured every 30 min for 3 h.

2.3. UV light response tests

The UV photodetector was irradiated with 365 nm ultraviolet light. The power of the UV irradiation was then limited to a low value of 90 mW/cm2 by means of the UV power control device.. This UV light irradiates vertically the sample surface in a dark test chamber, where the photocurrent signal is then detected using the precision source/measurement unit. This method involves real-time measurement using a two-point probe. The input voltage for the two-point measurement was set at 5 V.

2.4. Characterization techniques

Structural analysis of ZnO and ZLO thin films will be carried out using an X-ray diffractometer (MiniFlex600) with Cu Kα radiation, 0.15418 nm). Their microstructure was assessed using a scanning electron microscope (SEM) (TESCAN_VEGA3), while their intrinsic properties were evaluated using a Perkin Elmer fluorescence spectrometer (LS 45) with an excitation wavelength of 290 nm. The optical properties were evaluated by measuring transmittance spectra via UV–Vis SpectroScan 80D in the 190–1100 nm spectral range. For thermoelectrical testing, measuring the Seebeck coefficient was carried out by heating the two tips, serving to measure the potential difference, and measuring the temperature between the tips using thermocouples, or the temperature difference from 0 K to 120 K with an interval of 20 K.

3. Results and discussion

3.1. Structure analysis

Fig. 1 shows the XRD spectra of the $Zn_{1-x}La_xO$ thin films [x = 0, 2, 5, 10, and 15at. %]. From the spectra, it can be seen that all the films have a polycrystalline nature, as peaks located at 2θ = 31.956°, 34.637°, 36.415°, 47.783°, 56.634°, 62.962°and 67. 975°, corresponding respectively to the crystal planes of the (1 0 0), (0 0 2), (1 0 1), (1 0 2), (1 1 0), (1 0 3), and (1 1 2) hexagonal wurtzite structure conforming to the standard map number JCPDS (JCPDS 36-1451) [24–26]. Typically, the maximum intensity along (0 0 2) for undoped and 2% La-ZnO films, is apparent in the growth of the films that are preferentially oriented in the c-axis direction. In the case of 5% La-ZnO, 10% La-ZnO and 15% La-ZnO films there are 3 preferential orientations (1 0 0), (0 0 2), and (1 0 1), however, for the 15% La-ZnO films the (1 0 1) plane shows a maximum intensity. An increase in the intensity of the (1 0 1) peak is observed with the increase of the doping content, confirming the incorporation of the La^{3+} ion in the ZnO lattice. The variation in preferential orientation decreases progressively in La-ZnO films from doping levels of 5at.%, accompanied by a decrease in the intensity of peak (0 0 2) and a strengthening of peaks (1 0 0) and (1 0 1). This is explained by the initial nucleation on the substrate, which could be influenced by the incorporation of La^{3+} ions into the Zn^{2+} sites of the ZnO lattice. Neither the secondary phase of La_2O_3 oxides nor other phases are detected, this signifies a good dilution of the lanthanum ions in the ZnO lattice.

It can be seen that the position of the peaks is not exactly the same for all concentrations, there is a small shift of the peaks (1 0 1) towards a small angle in the case of the 10% La-ZnO and 15% La-ZnO films compared to pure ZnO, which informs us about the change of the lattice parameters with the introduction of lanthanum [27]. In addition, there is a progressive loss of crystallinity by increasing the concentration of lanthanum in the ZnO lattice, which results in a decrease in the intensity of the (0 0 2) peak.

The X-ray diffraction spectrum was used to determine the structural parameters of Zn1-xLaxO thin films [x = 0, 2, 5, 10, and 15 atm.%], such as lattice parameters (a and c) [28], The c/a ratio, the unit cell volume (V)[29], the lattice strain (ε), and the crystallite size (D), the latter calculated by applying the Debye-Scherrer formula [30], using the following equations, respectively:

$$\frac{1}{d_{hkl}^2} = \frac{(h^2 + k^2)}{a^2} + \frac{l^2}{c^2} \quad (1)$$

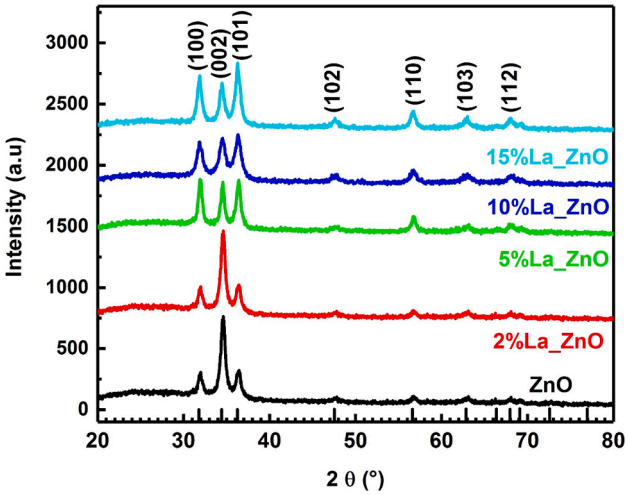

Fig. 1. XRD patterns of ZnO, Zn1-xLaxO[x = 2, 5, 10, 15 at.%] films deposited at 450 °C.

$$V = \frac{\sqrt{3}}{2}a^2c = 0.866a^2c \quad (2)$$

$$\varepsilon = \frac{\beta}{4\tan\theta} \quad (3)$$

$$D = \frac{0.9\lambda}{\beta\cos(\theta)} \quad (4)$$

where K is the dimensionless constant = 0.9, λ is the wavelength of the incident X-ray (Cu Kα radiation, λ = 1.5418 Å), β is the full width at half maximum (FWHM) of the diffraction peak, θ is the position of the considered diffraction peak (in radians), d_{hkl} the distances are expressed in [Å] and the angles in radians. The calculated values listed in Table 1. it can be seen that the lattice parameters (a and c) and cell volume of ZnO increase with increasing lanthanum concentration from 5.1868 Å, 46.99 $Å^3$ for the pure ZnO films, to 5.2038 Å, 47.42 $Å^3$ in the case of 15 at.% doped ZnO, this may be explained by the large difference in the ionic radii of La^{3+} (1.06 Å) and Zn^{2+} (0.74 Å). Based on the Hume-Rothery rule (%Δr > 15%) [31], La^{3+} ions do not introduce in a substitutional form, while lanthanum ions occupy the interstitial sites or available voids in the ZnO crystal lattice [32]. In addition, the value of the lattice strain (ε) decreases with doping which leads to a deformation of the elemental lattice in the form of compressive or dilational stresses, which in our case will be dilation (negative stresses) because 2θ is moving towards the small angles, due to the larger radius of La^{3+}. After 5% La-ZnO, the XRD pattern does not show a single preferential orientation, indicating a distortion of the crystal lattice in the La-doped ZnO. In addition, the c/a ratio value for the wurtzite structure is considered to be 1.633 [33]. For the present sample, the c/a ratio ranges from 1.6035 to 1.6053, indicating the formation of oxygen at the interstitial sites and zinc vacancies (V_{Zn}).

The crystallite size is the same for the 2%LZO films (15 nm) as for pure ZnO films (15 nm), then there is an increase in crystallite size for the 5% LZO films (19 nm). The reduction of the crystallite size was observed for the doping rate of 10% LZO films (10 nm) and then increases for 15%LZO films (16 nm). The decrease of the crystallite size for elaborated films is, probably, caused by the emergence of other growth planes at the expense of the (0 0 2) orientation used for the calculation of the crystallite size.

3.2. Microstructural observations

Fig. 2 shows the SEM images of the ZnO and LZO samples [2, 5, 10, 15at%]. The morphology of ZnO and 2%LZO layers covered with nanorods with a length of about 1 μm. are grown along the direction perpendicular to the substrate, which is consistent with the highly oriented ZnO (0 0 2) in the XRD patterns. It can be seen that the surface improved with doping, for 5%-LZO, 10%-LZO, and 15%-LZO The nanocrystals were hexagonal prisms with clearly distinct edges and corners, with smooth faces, with llengths1 μm grown in the direction along the (1 0 0), (1 0 1) plane in parallel with the substrate surface. Note that the nanorods diameter is increased with the increase of doping rate 0.25, 0.32, 0.40, 0.67 μm, for LZO [2, 5, 10, and 15at.%] respectively. These findings support the X-ray diffraction results and further, confirm the incorporation of La^{3+} ions into the ZnO lattice. It can be concluded that lanthanum doping significantly improves the morphology of ZnO.

Table 1
Structural parameters (cell parameters 'a' and 'c', c/a ratio, the average crystallite size (D), volume (V), and micro-strain (ε)) of ZnO and LZO thin films.

x% La	Cristallite Size (nm)	Lattice Parameters (nm)	c/a	Unit cell volume (nm^3)	ε %
0	15	a = 0.32344 c = 0.51868	1.6036	46.99×10^{-3}	−0.381
2	15	a = 0.32344 c = 0.51868	1.6036	46.99×10^{-3}	−0.381
5	19	a = 0.32354 c = 0.51937	1.6053	47.08×10^{-3}	−0.250
10	10	a = 0.32404 c = 0.51960	1.6035	47.25×10^{-3}	−0.204
15	16	a = 0.32438 c = 0.52038	1.6042	47.42×10^{-3}	−0.054

3.3. Optical properties

The optical transmission and reflectance spectra spectra of the elaborated thin films recorded at room temperature in the range of 200–1100 nm are shown in Figs. 3 and 4 respectively. The average transmission was observed from 80% to 90% in the visible range as the concentration of Lanthanum increases, where the transmittance shows a series of interference bangs due to multiple reflections in the ZnO and LZO layers. According to these findings, it is evident that doping with Lanthanum (10, 15 at.%) helps the improvement of transmission in the visible region. This demonstrates that this material can be used as a transparent oxide in solar cells.

The different values of the dispersion parameters of our samples such as d, Eg, n at 598 nm, and n∞ was estimated by a single effect oscillator fit, suggested by Wemple and DiDomenico [34], are listed in Table 2.

The determination of the optical gap Eg is based on the model proposed by Tauc plot [1,22,25].

$$\alpha h\upsilon = A\left(h\upsilon - E_g\right)^{1/2} \quad (5)$$

A is a constant, Eg is the optical bandgap expressed in eV, E = hυ is the energy of the photon in eV. Plotting $(\alpha h\upsilon)^2$ as a function of the energy of a photon ($E = h\upsilon$) and by the extrapolation method, the intersection of the tangent with the x-axis (for $((\alpha h\upsilon)^2 = 0)$, represents the optical gap *Eg*. The optical bandgap values show considerable stability, as shown in Table 2, from 3.26 eV for the undoped layer [34,35], to 3.27 eV, 3.26 eV, 3.26 eV, 3.26 eV for the layer doped with 2%LZO, 5% LZO, 10%LZO, 15%LZO. However, these values are lower than those for bulk ZnO (3.31 eV) [36]. In this study, the deformation of the crystal lattice, modification of the electronic structure and reduction of the average grain size do not influence the optical gap values [35]. This confirms that the La^{3+} ion is introduced into the interstitial sites.

Fig. 5 shows the refractive index values calculated from experimental data [34], which is recorded in Table 2, and it is known that an inverse relationship exists between refractive index and transmittance. In our study, we found the following results: as the doping rate increases, refractive index values increase and transmittance values decrease 1.82 (86%), 1.83 (80%), 1.84 (86%), 1. 77 (90%), 1.82 (87%) for thin ZnO layers, 2%LZO, 5%LZO, 10%LZO, 15%LZO, these results can be interpreted by a relationship between crystal structure and transmittance, i.e. there's a relationship to the growth direction c (0 0 2), as peak intensity (0 0 2) increases, the transmittance decreases and the refractive index increases as a result of the incorporation of La3+ ions into the ZnO lattice. On the other hand, film thickness values are presented in Table 1, which increase for a doping level of 2%LZO (368 nm), then decrease with increasing doping levels of 367, 357, 300, 259 nm for the ZnO layer, 5%LZO, 10%LZO, 15%LZO respectively. This can be interpreted as thickness saturation at 2%LZO [37].

3.4. Photoluminescence spectra analysis

Photoluminescence properties were studied using an LS45 spectrophotometer in the 350–700 nm range. The emission spectra of the processed layers were recorded at room temperature with an excitation wavelength of 290 nm and are shown in Fig. 6a. All spectra are characterized by 2 emission bands. A blue emission band around 413 nm (2.99), 415 nm (2. 98 eV), 409 nm (3. 02 eV), 412 nm (3. 00 eV), and 410 nm (3. 01 eV) for the ZnO, 2% La_ZnO, 5% La_ZnO, 10% La_ZnO,

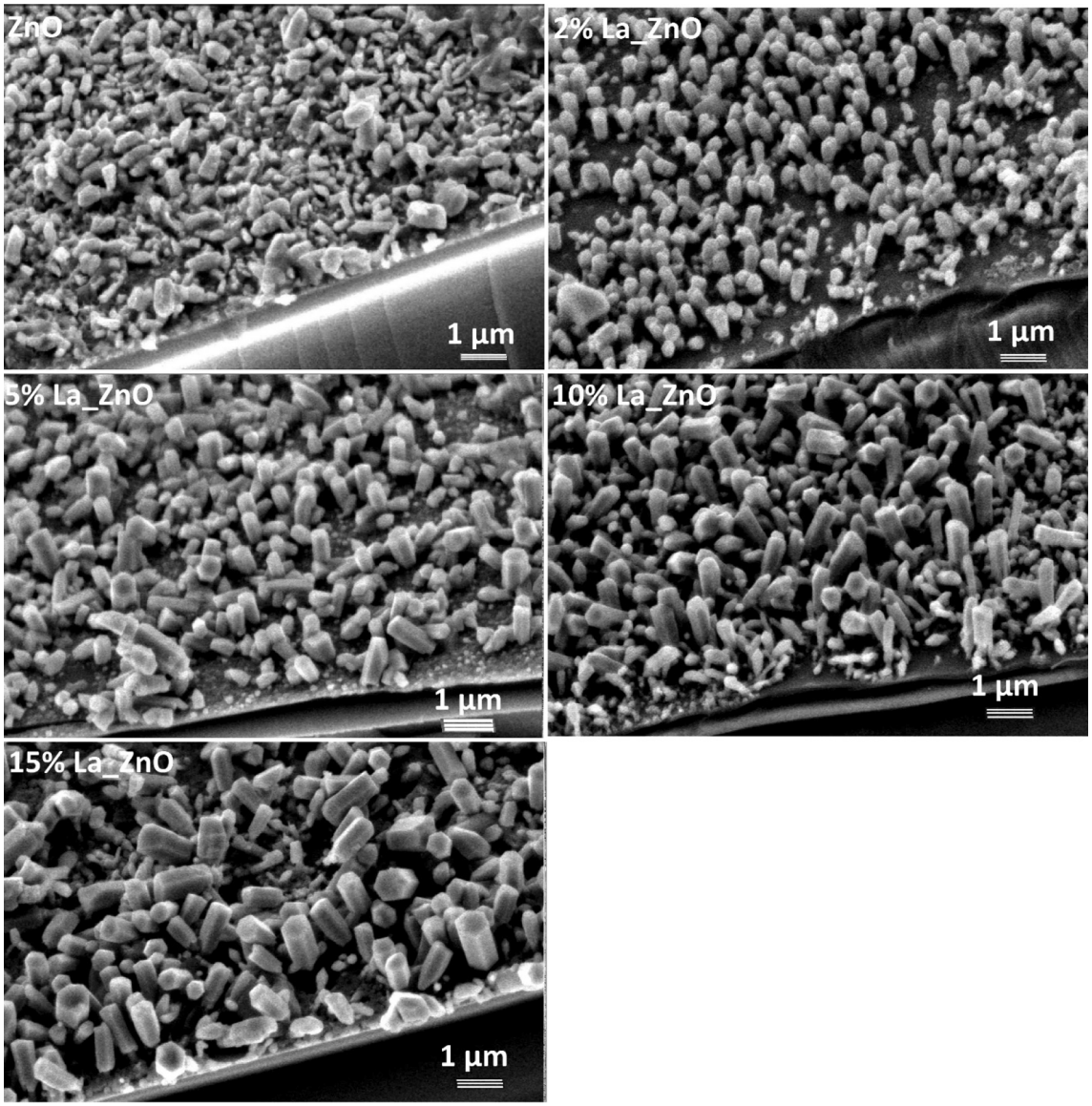

Fig. 2. SEM images of ZnO, Zn1-xLaxO[x = 2, 5, 10, 15 at.%] films deposited at 450 °C.

and 15% La_ZnO layers respectively, which can be assigned to near-band edge (NBE) emission from free exciton recombination and excitons [38], the Gaussian peaks (dashed lines) are shown at the bottom of Fig. 6b, while the solid line represents the linear combination of the multi-Gaussian peaks with a constant background. The Gaussian peak position, area, width (nm), and height (a. u) are shown in the inset of Fig. 5b. mathematical treatment of the PL intensity there is a slight shift in band position to 412.48 ± 3. 12 nm (E = 3.00 ± 0.02 eV) due to the introduction of La^{3+}. On the other hand, this slight shift towards the long (short) wavelengths of the band-to-band transition is accompanied by a slight decrease (increase) in the optical gap, and in our study we find that the values of the optical gap energy remain constant at a value of (3.26 eV), except for the 2%LZO films, which confirms that the La^{3+} ions introduced into the eastern sites are not in substitution. The low intensity of the 15%LZO films shows that the rate of recombination of electron-hole pairs becomes lower after the introduction of La atoms, i.e. photogenerated electrons are trapped at the energy levels created by defects in the band gap.

The second, a broader emission in the visible around 483 nm (2.56), 489 nm (2. 53 eV), 509 nm (2. 43 eV), 496 nm (2.49 eV), and 483 nm (2. 56 eV) for ZnO, 2% La_ZnO, 5% La_ZnO, 10% La_ZnO, and 15% La_ZnO layers respectively, linked to intrinsic defects and impurities in ZnO such as oxygen voids (Vo), zinc voids (VZn), oxygen (Oi) and zinc (Zni) interstitials, dopants [39,40]. From Fig. 5b. shown that a band offset of 492. 50 ± 9. 50 nm (E = 2.52 ± 0.08 eV). The presence of these emissions confirms the existence of oxygen vacancies on the surface of the ZnO catalyst. The observed emission at 492.50 ± 9. 50 nm has been ascribed to the oxygen vacancies (Vo) transition to oxygen interstitials (Oi) [41,42], where the valence oxygen vacancies have been ionized [43] and linked to zinc vacancies (V_{Zn}) and oxygen vacancies (Vo) [44]. In contrast, recombination of the electron-hole pair is usually characterized by localized states with energy levels within the band gap, producing lower-energy emission [45].

Their emission intensity improves with the doping level, with maximum values achieved for the 2%LZO and 10%LZO films, possibly as a result of the increase in deflections on the ZnO surface, and the presence of a high concentration of oxygen vacancies and other defects, which explicit by a higher separation rate of photo-induced charge carriers, the higher separation between the photoelectrons and holes [46].

For the 5%LZO films, the intensity of emission is lower than that of 2%LZO and 10%LZO, but at the same time higher than that of ZnO;

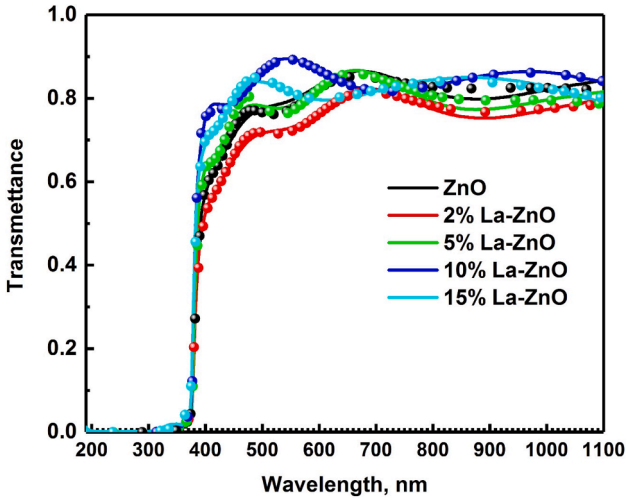

Fig. 3. Transmission spectra of ZnO, LZO thin films deposited on glass substrate at 450 °C. Measured (full circles) and calculated (solid lines) transmittance spectra of films.

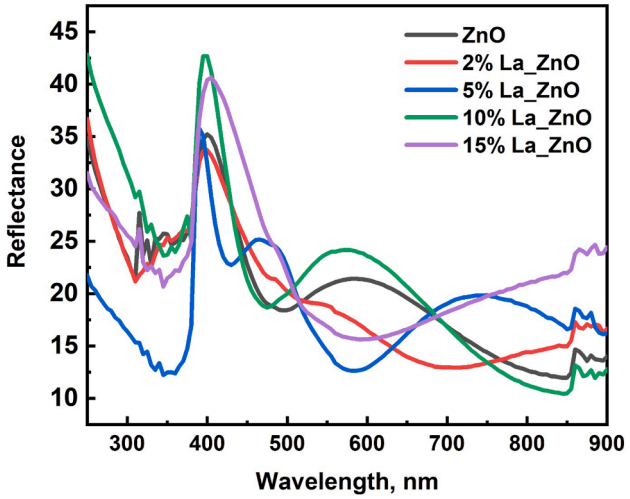

Fig. 4. Reflectance spectra of ZnO, $Zn_{1-x}La_xO$[x = 2, 5, 10, 15 at.%] films deposited at 450 °C.

Table 2
Dispersion parameters of the La_ZnO films extracted by fitting the experimental data.

Samples	Thickness (nm)	Eg (eV)	n at 598 nm	n_∞
ZnO	367	3.26	1.82	1.74
2%La_ZnO	368	3.27	1.83	1.72
5% La_ZnO	357	3.26	1.84	1.74
10% La_ZnO	300	3.26	1.77	1.70
15% La_ZnO	259	3.26	1.82	1.74

whereas the emission intensity of the 15%LZO films is less than that of ZnO. a fact that is consistent with the results of XRD, SEM, and photocatalysis.

3.5. Seebeck coefficient

The term "thermoelectricity" refers to a physical phenomenon that occurs in a conductor or semiconductor when it is exposed to a temperature difference or when a current flows through it. In materials, there are basically three thermoelectric effects: the Seebeck, Peltier and Thomson effects [47]. The Seebeck effect refers to the flow of current due to the temperature gradient between the two ends of a material. Fig. 7. A graphical representation of ΔV versus temperature gradient for LZO films from 0 to 120 K.

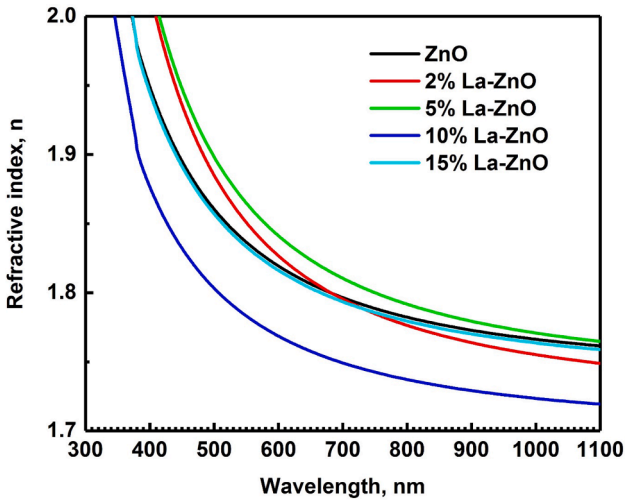

Fig. 5. Refractive index of ZnO, LZO thin films deposited onto glass substrate at 450 °C.

The Seebeck coefficient (expressed in mV/K) is calculated from the following relationship [48].

$$S = -\frac{\Delta V}{\Delta T} \tag{6}$$

where ΔV is the offset voltage measured when the temperature difference ΔT between the two tip contacts on the sample (Vhot tip - Vcold tip). The evolution of the thermoelectric coefficient being proportional to the temperature difference between the tips, the S values obtained are −319, −333, −366, −370 and −282 for ZnO, 2%LZO, 5%LZO, 10%LZO and 15%LZO respectively, the S values are negative for all films, which is characteristic of an n-type semiconductor (the free carriers are electrons in the case of) [1,48]. The fact that the Seebeck coefficient increases in absolute value for doping levels above 10% is evidence of competition between various phenomena, such as the incorporation of additional dopants and impurities creating more damage than true doping.

As the Seebeck coefficient is inversely proportional to the carrier concentration [49], the carrier concentration was calculated using the following equations (7), together the effective density in the conduction band, determined using Eq (8) [50]., when |S|> 75 μV/K [51]:

$$m_S^* = \frac{h^2}{2k_BT}\left\{\frac{3n}{16\sqrt{\pi}}\left(exp\left[\frac{|S|}{(k_B/e)} - 2\right] - 0.17\right)\right\}^{2/3} \tag{7}$$

$$N_C = 2\left(\frac{2\pi m_S^* k_B T}{h^2}\right)^{3/2} \tag{8}$$

where e is the charge of the carrier, kB denotes Boltzmann's constant, T represents the absolute temperature, h is the Planck constant, mS* (mS*= 0.28 m_0) is the effective Seebeck mass of ZnO, and n represents the carrier concentration. The results of carrier concentration of the ZnO, LZO thin films are shown in Fig. 8. the values of carrier concentration increased with doping level from 5.95 × 10^{17}, 4.9810^{17}, 3.3910^{17}, 3.2110^{17}, 9.1810^{17} cm^{-3} for ZnO and $Zn_{0.98}La_{0.02}O$, $Zn_{0.95}La_{0.05}O$ $Zn_{0.90}La_{0.10}O$, $Zn_{0.85}La_{0.15}O$ films respectively. In addition, the calculated effective density of ZnO was 3.71 × 10^{18} cm^{-3}, and we note that our ZnO, LZO layers were non-degenerate, which explains the optical results (the stable Eg values).

The Fermi energy level (FE) can be calculated using the following

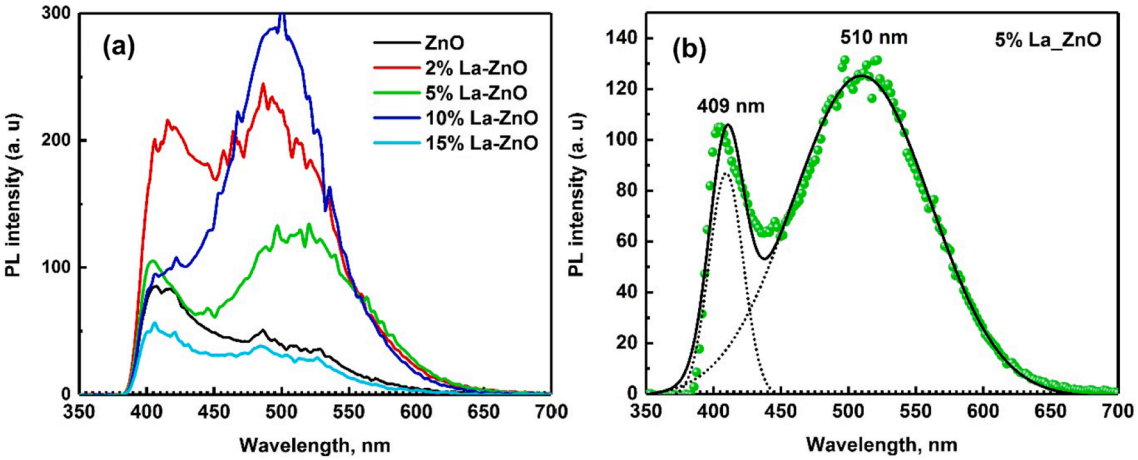

Fig. 6. A) Photoluminescence spectra of ZnO and LZO films and b) The Gaussian deconvolution of the PL intensity of $Zn_{0.95}La_{0.05}O$ films deposited on a glass substrate at 450 °C.

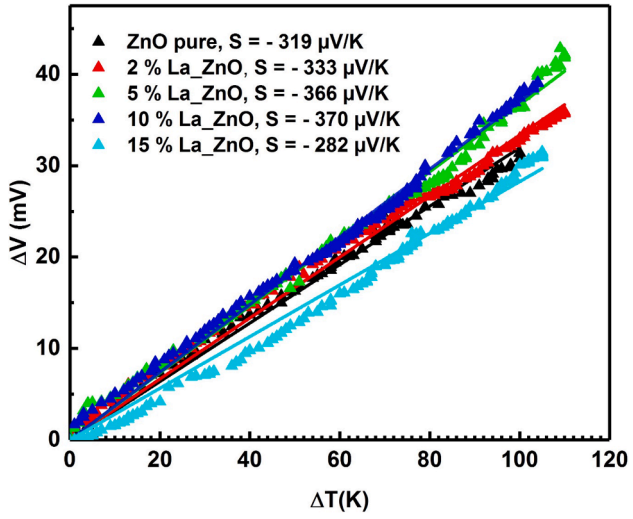

Fig. 7. Seebeck coefficients for ZnO, and La-doped ZnO thin films with different La concentrations.

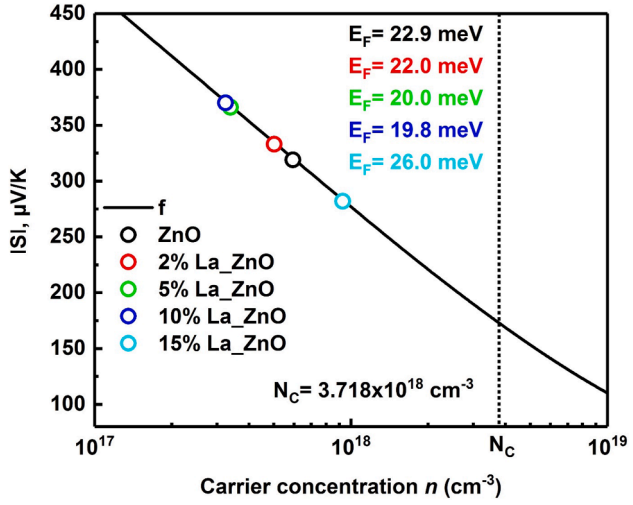

Fig. 8. Seebeck coefficients as a function of carrier concentrations for ZnO and LZO thin films.

equation [47].

$$E_F = \frac{\pi^2 k_B^2 T}{3|e||S|} \quad (9)$$

Fig. 8 shows the Fermi energy values. These decrease with increasing dopant content, which could be interpreted as La^{+3} diffusion into the ZnO lattice, as La^{+3} ions introduced into interstitial sites will generate additional electron vacancies. Except for films containing 15% LZO, due to the increase in the number of electrons (i.e. charge carriers) that are promoted above the Fermi level in the conduction band as a result of the increase in La^{3+} ions.

3.6. UV photodetector

Fig. 9 shows the photocurrent of the $Zn_{1-x}La_xO$ films [x = 0.0, 0.02, 0.05, 0.10, 0.15] in the dark and under UV light with the interval 30 s, under + 5 V voltage. It is observed that all films show the transient response of the measured current with switching on and off UV illumination. The spectrum revealed that the photocurrent decreases monotonously with increasing La conten. It's conventional that the photoresponse mechanism of ZnO-based UV PDs, where oxygen molecule adsorption and desorption play a crucial role in photoconduction. In the dark, oxygen molecules adsorbed on the ZnO surface from the ambient atmosphere according to the equation:

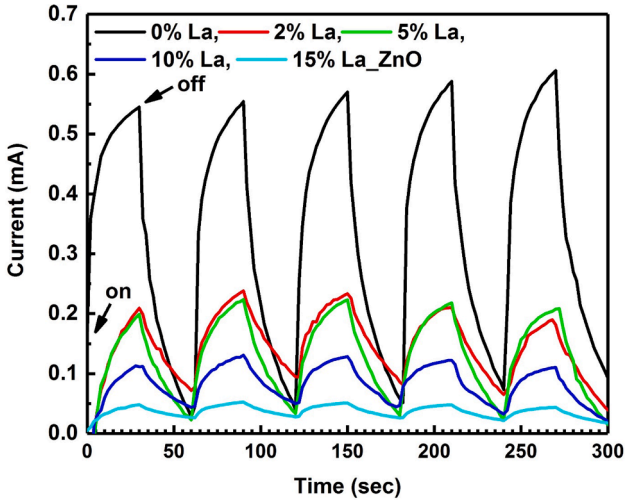

Fig. 9. UV response during 5 UV on–off sensing cycles for ZnO and LZO samples at a UV intensity of 1500 mW/cm^2.

$$O_2(gaz) + e^-(surface) \rightarrow O_2^-(adsorption) \quad (10)$$

And then form a low conductivity depletion region, under exposure to UV illumination, e^-–h^+ pairs are photogenerated, where some of the photogenerated holes desorb the adsorbed oxygen molecules from the ZnO surface to decrease the low conductivity depletion width as follows,

$$h^+ + O_2^-(adsorption) \rightarrow O_2(gaz) \quad (11)$$

Finally, the unpaired photogenerated free electrons together with available holes contribute to photoconduction in the presence of an external driving force [52,53].

Fig. 10 shows I-V properties of ZnO and LZO film photodetectors in the dark (dark current) and at 365 nm irradiation (photocurrent), the values are presented in Table 3, observed that the La-doping can reduce the dark current and enhance the electrical properties, For the dark current of ZnO obtained are 6.4×10^{-4} A this value is very important compared to 2.92×10^{-7} A obtained by T. P. Chen et al [54]. In addition, the photocurrent of our ZnO sample is 2.23×10^{-3} A is very highest than 7.32×10^{-6} A of the photocurrent of the ZnO MSM UV sensors with Ag and Pd contact electrodes fabricated by S.J. Young et al [55].

The sensitivity values of the $Zn_{1-x}La_xO$ films [x = 0.0, 0.02, 0.05, 0.10, 0.15] PD, are given in Table 3, and we note that the 15%La-ZnO layers are more sensitive but with a lower current, while the 5%La-ZnO layers have a good sensitivity compared with the other layers, and even pure ZnO. These results are in agreement with those obtained in the photocatalysis section. Other studies show that in the ZnO: Ag films, the sensitivity is increased with the increase of silver content, the concentration of carrier increases and reduces the refractive index of ZnO [56]. However, Yen-Lin Chu et al [57], report that Ga-ZnO thin films produced by simple chemical methods at room temperature have significantly higher photo-responsivity and stability than undoped ZnO PDs exposed to 380 nm UV illumination with an applied bias of 3 V.

In Table 4, a comparison of the highest value obtained from 5%La-ZnO versus other doped ZnO layers reveals that this layer is more sensitive than the In-doped layer, while FZO layers prepared by Yen-Lin Chu et al [58] show better sensitivity than IZO [59] and LZO layers.

It can be seen that with increasing time, thin layers of 5%LZO are better photogenerated than other LZO layers. So many factors influence the photodetector of LZO films, the incorporation of La in the ZnO lattice changes the preferential orientation, and surface morphology, car the amount of La occupies the vacuum of oxygen (PL), and this variation in the surface morphology affects the adsorption of oxygen, However, LZO thin films are particularly suitable for detecting UV light.

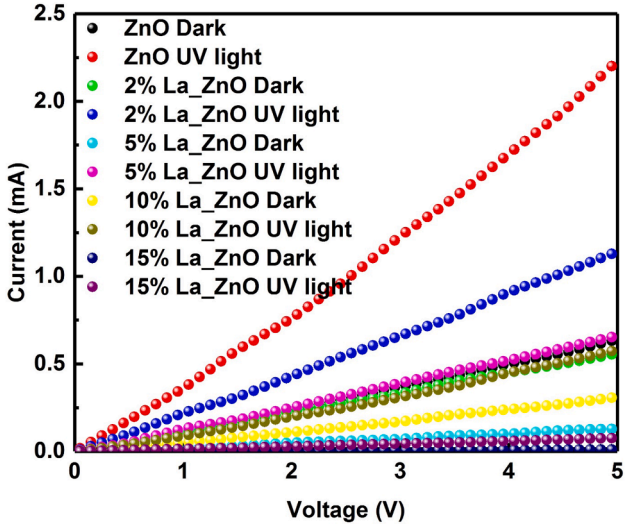

Fig. 10. The I-V curves of ZnO and LZO samples measured in the dark and under UV illumination.

Table 3
The results exhibited the parameters of the prepared ZnO samples with and without La content at 5 V.

Samples	I_{dark} (mA)	I_{photo} (mA)	Sensitivity
Pure ZnO	0.64	2.23	3.48
2%La_ZnO	0.56	1.14	2.03
5%La_ZnO	0.13	0.66	5.07
10%La_ZnO	0.31	0.58	1.87
15%La_ZnO	0.0117	0.0765	6.53

Table 4
Some results of doped ZnO PD films.

Samples	Sensitivity	λ (nm)	Voltage (V)
LZO	5.07	365	5
FZO	471.1 [58]	380	3
IZO	2.5 [59]	390	1

3.7. The photocatalytic performance of the La-doped ZnO thin films

Rare earth (RE) are elegant dopant for the photodegradation of organic pollutants. Recently, the rare-earth-doped photocatalyst has received a lot of attention. The unique photocatalytic and redox properties of RE are important for promoting the surface properties and electron transfer activity of the photocatalyst. ZnO doped with La exhibits enhanced photocatalytic activity compared with undoped ZnO [60,61]. Photodegradation of aqueous methylene blue solution (8.10–2 M) under UV light irradiation for 3 h, using ZnO thin films, $Zn_{1-x}La_xO$ [2, 5, 10, 15at.%] was studied. Fig. 11. shows the optical absorption spectra of MB after UV irradiation at different exposure times for all ZnO, and LZO films, recorded in the range of 500 to 750 nm. A decrease in the maximum absorbance observed at 663 nm as a function of time can be seen for all films, confirming the degradation of MB.

Our results show that there is no proportional relationship between the absorption rate and the doping rate. It is clear that 10%LZO thin films have low absorption than pure ZnO layers, whereas 15%LZO and 5%LZO layers improve degradation more evenly than ZnO, and the 2% LZO layers have a medium absorption rate.

The decrease in maximum absorbance observed at 663 nm as a function of time, can be used to quantify the degradation rate D_r (%) of MB using the following relation.

$$D_r\% = \left[1 - \frac{A_t}{A_0}\right] \times 100 \quad (12)$$

where A_t and A_0 are the absorption of the MB solution at 663 nm after irradiation during and before irradiation, respectively. Fig. 12 shows the rate of degradation as a function of time.

A high degradation rate, around 96%, is observed for films prepared from 5%LZO versus pure ZnO (86%). And an 87% degradation rate for 15%LZO films. However, 10%LZO thin films show a low degradation activity of around 34%. The 2%LZO films had a good degradation rate of 74%. The photocatalytic efficiency of the films increases with increasing La^{3+} ions concentration but stabilizes at 5at%(La). Therefore, it can be concluded that the optimum catalyst concentration is 5at. %.

In order to describe the photodegradation reaction kinetics of dyes at low concentrations, the apparent photocatalytic reaction rate constant K was calculated by representing the photodegradation ratio from Fig. 13 in terms of the following pseudo-first-order equation [62].

$$A = X^*exp(-k^*t) + E \quad (13)$$

While the k-order (pseudo) rate constant is the inverse of that of the time used (min- 1), the X represents the amplitude of the process, and E corresponds to the end point, both in the same units as the measured value A. As shown by the values recorded in Table 5, the values of R^2 = 0.9990, 0.9953, 0.9960, 0.9788, 0.9971 for the ZnO, 2%LZO, 5%LZO,

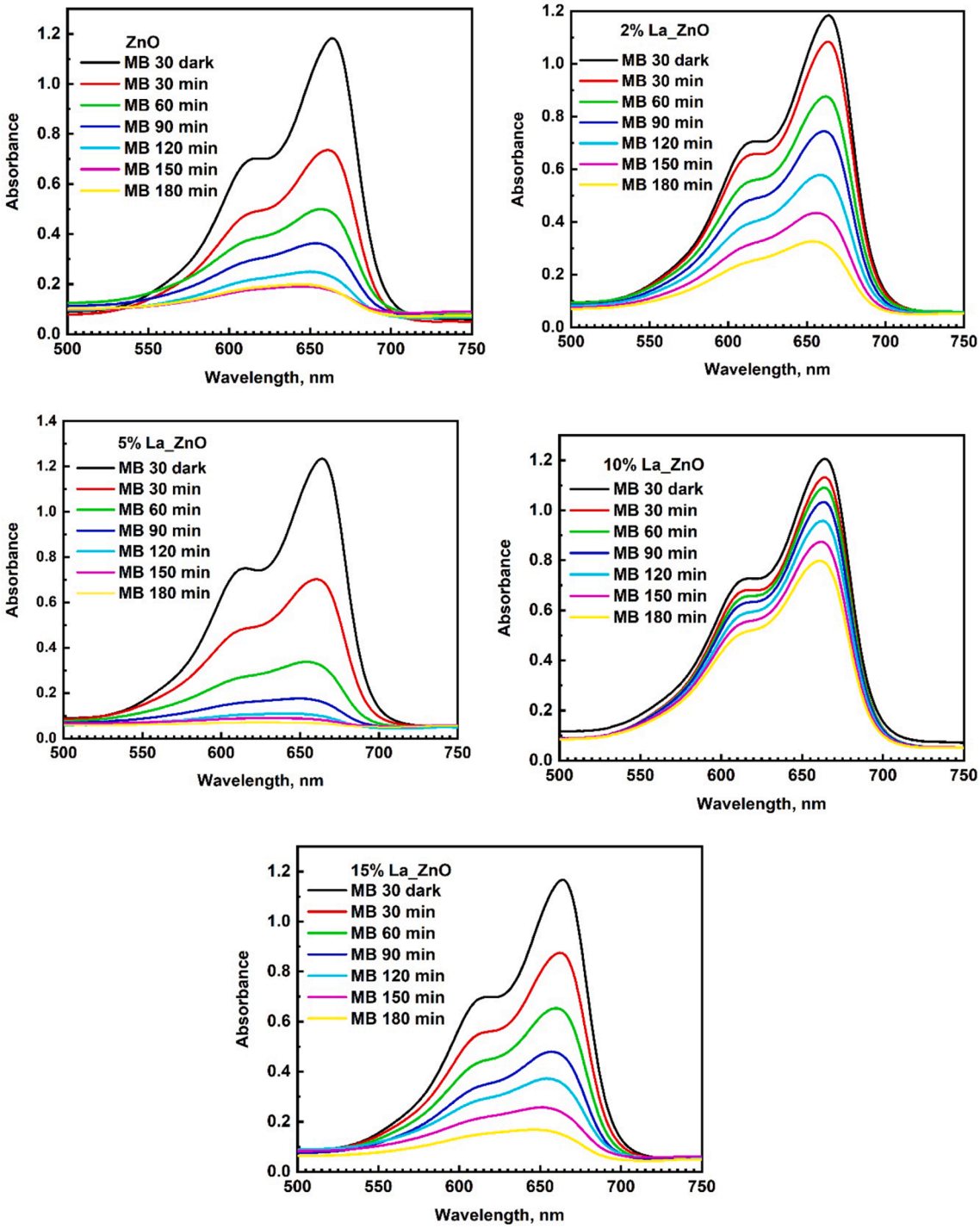

Fig. 11. Photocatalytic activity of ZnO and LZO thin films in MB solution under UV irradiation for different reaction time.

10%LZO and 15%LZO layers respectively indicate that the photocatalytic reaction for all films is a first-order reaction.

The values of the rate constant k for the thin films were as follows: ZnO (0.53221 min^{-1}), 2%La_ZnO (-0.00441 min^{-1}), 5%La_ZnO (0.67120 min^{-1}), 10%La_ZnO (−0.0975 min^{-1}), 15%La_ZnO (0.53006 min^{-1}), an irregular variation of the rate constant k for thin films (0.0084 min^{-1}), an irregular variation of the kinetic constant with La concentrations is obtained. The maximum value is obtained for films with 5%La_ZnO. This result is due to the presence of a large number of oxygen vacancies [63], which enhance the center of activity, thus helping to increase photocatalysis efficiency. In addition, more surface defects are present, causing the creation of a contact zone on the surface of ZnO films that separate the recombination of photogenerated electrons and holes, resulting in enhanced photocatalytic activity.

Fig. 14 summarizes the mechanisms of MB photodegradation by ZnO and LZO [2, 5, 10,15 at.%] films semiconductor irradiated with energy UV-light. In general heterogeneous photocatalysis is a catalytic process based on the excitation of a semiconductor (ZnO) by light radiation with a wavelength below 390 nm corresponding to an energy greater than or equal to the band gap of 3. 30 eV, leading to accelerated photoreaction involving reactions between electron/hole pairs and organic and inorganic products adsorbed on the semiconductor surface. This absorption

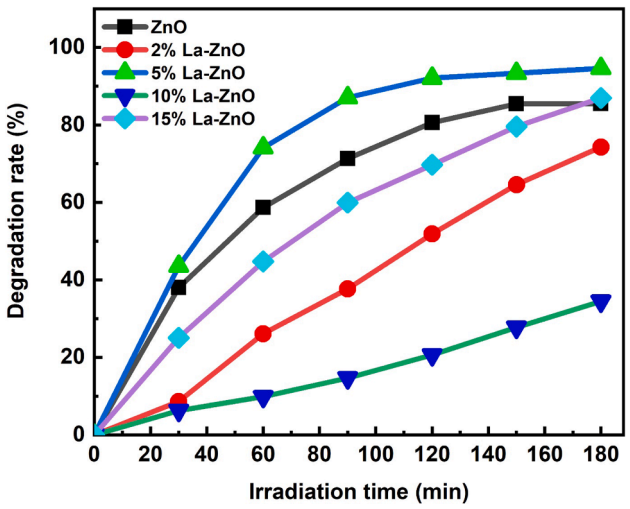

Fig. 12. Degradation rate of ZnO and LZO films in MB solution.

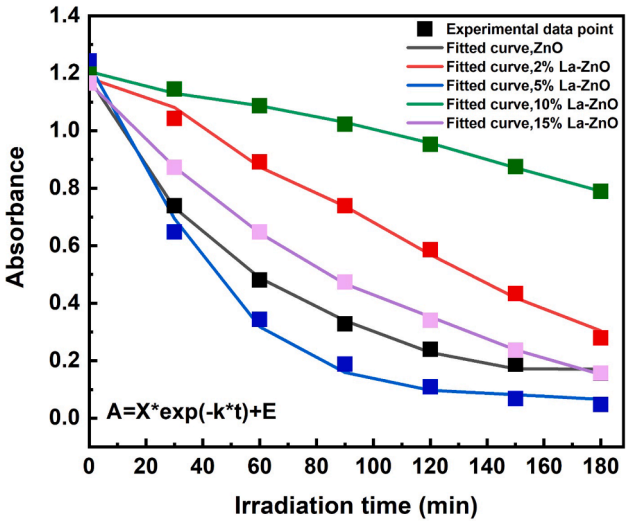

Fig. 13. Degradation kinetics of MB aqueous solutions by ZnO and LZO films.

results in the activation of the semiconductor (ZnO). Under light excitation, electrons (e^-) in ZnO valence band (VB) move into the conduction band (CB), leaving a positive charge or hole (denoted h^+) in the VB. The carrier pairs (e^-/h^+) then migrate to the surface of the catalyst (ZnO). Photo-generated electrons and holes can then recombine simultaneously at a rate dependent on several factors related to the photocatalytic structure and surface modifications. This effect essentially depends on the photocatalyst, such as its nature, concentration, Ph, and type of doping [64].

$$ZnO + h\upsilon(UV) \rightarrow e^- + h^+ \quad (14)$$

An indispensable property of lanthanum is its ability to capture photogenerated electrons according to equation (15):

$$La^{3+} + e^- \rightarrow La^{2+} \quad (15)$$

The lanthanum ion (La^{2+}=[Xe] $5d^1$) ends up with an additional 5d electron orbital. La^{2+} tends to return to their stable configurations with the 3 + oxidation states (La^{3+} = [Xe]). This can be achieved by transferring the trapped electron to the oxygen molecule O_2 as follows.

$$La^{2+} + O_2 \rightarrow La^{3+} + O_2^{\bullet} \quad (16)$$

The superoxide radical produced ($O_2^{\bullet}$) is responsible for generating •OH radicals, known as highly reactive electrophilic oxides.

$$O_2^{-\bullet} + H^+ \rightarrow {}^{\cdot}OOH \quad (17)$$

$${}^{\cdot}OOH \rightarrow H_2O_2 + O_2 \quad (18)$$

$$H_2O_2 + e_{CB}^- \rightarrow OH^- + {}^{\cdot}OH \quad (19)$$

Photo-generated holes can react with H_2O molecules to produce •OH radicals:

$$h_{VB}^+ + H_2O \rightarrow H^+ + {}^{\cdot}OH \quad (20)$$

The doping of ZnO with La serves to considerably improve its catalytic properties by modifying the surface state of the ZnO. This can be seen in the large number of defects generated, notably oxygen gap sites [65–67], which serve to trap electrons and subsequently produce a quantity of radicals (–OH) that will raise the pH of the solution to an optimum, which has been estimated at around 10 [68].

In this study, we found that there is no fixed relationship between the catalytic properties of LZO and other structural, microstructural, and optical properties. A number of studies [65–67], show that particle size reduction (large specific surface area) is suggested to decrease the probability of recombination of electron-hole pairs (e−/h+), which in turn improves photo-catalytic activity, but this trend does not apply in our case, ZnO (15 nm, Dr = 86%), 2%LZO (15 nm, Dr = 74%), 5%LZO (19 nm, Dr = 96%), 10%LZO (10 nm, Dr = 34%), and 15%LZO (16 nm, Dr = 87%). Thus, the variation in optical gap energy cannot be interpreted as lanthanum doping does not affect Eg, which has a fixed value of 3.26 eV. Our results show that lanthanum doping influences the microstructure of ZnO, confirming that photodegradation efficiency can be improved through the evolution of the ZnO structure. The doping of ZnO with La serves to considerably improve its catalytic properties by modifying the surface state of the ZnO. This can be seen in the large number of defects generated, notably oxygen gap sites [68–70], which serve to trap electrons and subsequently produce a number of radicals (–OH) that will raise the pH of the solution to an optimum, which has been estimated at around 10 [71]. Recently, ZnO nanostructures have received great interest for photocatalytic study due to their unique promising characteristics. Nanostructured ZnO can exist in various morphologies such as, one-dimensional (1D) nanostructures (nanowires, nanorods, nanotubes…), two-dimensional (2D) and three-dimensional (3D) (nanodisk, nanoflower like nanocube, Nanoursins), where are different surfaces, polar planes or oxygen vacancies [72].

Table 5
Pseudo-first-order kinetic parameters of MB degradation.

Samples	Value			Standard deviation			R^2
	K(min^{-1})	X	E	K(min^{-1})	X	E	
ZnO	0.53221	1.06674	0.1127	0.02140	0.02140	0.0135	0.9990
2% La-ZnO	−0.00441	−34.038	35.231	0.03514	274.453	274.46	0.9953
5% La-ZnO	0.67120	1.21768	0.0254	0.05089	0.03511	0.0249	0.9960
10% La-ZnO	−0,0975	−0,5121	1,70945	0,02778	0,19315	0,1981	0.9788
15% La-ZnO	0.53006	1.27594	−0.11078	0.01015	0.02330	0.0252	0.9971

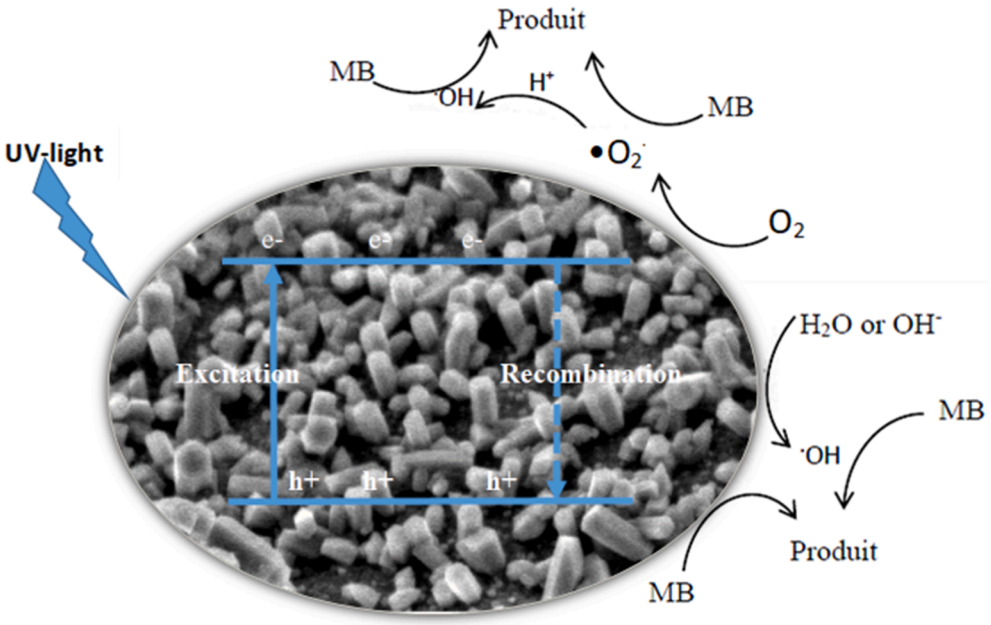

Fig. 14. Degradation mechanism of MB solution by ZnO and LZO films.

4. Conclusion

ZnO, $Zn_{1-x}La_xO$ [2, 5, 10, 15%] films were prepared by spray pyrolysis on a glass substrate at 450 °C for 1 h. XRD patterns confirmed the hexagonal wurtzite-like structure for the pure ZnO and LZO films, with the preferential orientation varying with increasing the La content, and the average crystallite size estimated at between 10 and 19 nm. The microstructure reveals that doping has affected the morphology. As regards optical properties, the transmittance value increased with increasing doping content, with a constant band gap energy value of 3.26 eV. As doping increased, the Seebeck coefficient changed. However, the maximum carrier concentration value is 9.18×10^{17} cm^{-3} for 15% LZO films. For UV photodetectors, we find that 5%La-ZnO films are more effective than ZOn films for UV photodetectors with high reactivity. Results from the photocatalytic application of methylene blue indicated that the 5%La_ZnO sample is more suitable for photocatalytic applications with a 95% degradation rate. Because of the excellent properties of the synthesized films: small crystallite size, well-defined morphology, and high transparency, they can be used as: optical windows in voltaic cells, polarizing substrates for photo-catalytic applications, gas sensors, heavy metal extraction (water decontamination) or in antibacterial applications. Based on this study, it was found that the relationship between UV photodetectors and photocatalysis depends on the surface of the sample, doping with lanthanum leads to structural defects and also influences oxygen vacancies, while 5%La-ZnO presents the best surface for UV photodetectors and photocatalysis.

Declaration of Competing Interest

The authors declare the following financial interests/personal relationships which may be considered as potential competing interests: [Sabrina Roguai reports was provided by Abbes Laghrour University of Khenchela Faculty of Science and Technology. Sabrina Roguai reports a relationship with Abbes Laghrour University of Khenchela Faculty of Science and Technology that includes: employment.].

Data availability

No data was used for the research described in the article.

Acknowledgements

Funding was provided by the General Direction of research and development technologies/ Ministry of Higher Education and Research Sciences DGRSDT/ MESRS, Algeria. The financial support from Abbes Laghrour University of Khenchela (Algeria). The authors would like to thank the Project (RFU) and LASPI^{2}A Laboratory of Khenchela University (Algeria) for their financial support of this research project.

References

[1] S. Roguai, A. Djelloul, Solid State Commun. 350 (2022), 114740.
[2] Y. Caglar, S. Aksoy, S. Ilican, M. Caglar, Superlattice. Microst. 46 (2009) 469–475.
[3] S. Anandan, A. Vinu, K.L.P. Sheeja Lovely, N. Gokulakrishnan, P. Srinivasu, T. Mori, V. Murugesan, V. Sivamurugan, K. Ariga, J. Mol. Catal. A Chem. 266 (2007) 149–157.
[4] G. Lucovsky, J.C. Phillips, Thin Solid Films 486 (2005) 200–204.
[5] K.L. Frindell, M.H. Bartl, M.R. Robinson, G.C. Bazan, A. Popitsch, G.D. Stucky, J. Solid State Chem. 172 (2003) 81–88.
[6] C. Mrabet, N. Mahdhi, A. Boukhachem, M. Amlouk, T. Manoubi, T,, J. Alloys Comp. 688 (2016) 122–132.
[7] H. Herrmann, J. Nolde, S. Berger, S. Heise, Ecotoxicol. Environ. Saf. 124 (2016) 213–238.
[8] M.A. Lahmer, Appl. Surf. Sci. 457 (2018) 315–322.
[9] D. Sridevi, K.V. Rajendran, Optoelectron Adv. Mater. 4 (2010) 1591–1593.
[10] J. Xu, S. Hao, X. Duan, S. Gu, X. Meng, J. Mater. Sci. Mater. Electron. 24 (2013) 4175–4179.
[11] J.S. Cho, Y.J. Kim, J.C. Lee, S.H. Park, K.H. Yoon, Sol. Energy Mater. Sol. Cells 95 (2011) 190–194.
[12] B. Wen, C.Q. Liu, N. Wang, H.L. Wang, S.M. Liu, W.W. Jiang, W.Y. Ding, W.D. Fei, W.P. Cha, Appl. Phys. A 121 (2015) 1147–1153.
[13] Y.F. Hsiou, W.K. Hung, C.W. Wang, Atlas J. Mater. Sci. 2 (2015) 60–64.
[14] X. Cai, H. Liang, X. Xia, R. Shen, Y. Liu, Y. Luo, G. Du, J. Mater. Sci. Mater. Electron. 26 (2015) 1591–1596.
[15] T. Morita, S. Ueno, T. Tokunaga, E. Hosono, Y. Oaki, H. Imai, H. Matsuda, H. Zhou, M. Hagiwara, S. Fujihara, Cryst. Growth Des. 15 (2015) 3150–3156.
[16] M. Suja, S.B. Bashar, M.M. Morshed, J. Liu, A.C.S. Appl, Mater. Interfaces 7 (16) (2015) 8894–8899.
[17] C.C. Yu, W.H. Lan, K.F. Huang, J. Nanomater. 2014 (2014) 1–4.
[18] J.C. Hsiao, C.H. Chen, H.J. Yang, C.L. Wu, C.M. Fan, J. Taiwan Inst. Chem. Eng. 44 (2013) 758–761.
[19] O.A. Novodvorsky, L.S. Gorbatenko, V.Y. Panchenko, O.D. Khramova, Y. A. Cherebilo, C. Wenzel, J.W. Bartha, V.T. Bublik, K.D. Shcherbachev, Semicond. 43 (2009) 419–424.
[20] R. Govindaraj, R. Govindan, M. Geetha, P. Anbarasan, Optik 126 (2015) 1555–1558.
[21] D.K. Vipin Kumar, P.A. Dwivedi, Sci. Sinter. 45 (2013) 13–19.
[22] S. Roguai, A. Djelloul, Appl. Phys. A 125 (2019) 816.
[23] S. Roguai, A. Djelloul, AJRESD. 4 (2022) 94–100.

[24] K.V. Chandekar, M. Shkir, A. Khan, B.M. Al-Shehri, M.S. Hamdy, S. AlFaify, M. A. El- Toni, A. Aldalbahi, A.A. Ansari, H. Ghaithan, J. Photochem. Photobiol. Chem. 395 (2020), 112465.
[25] S. Roguai, A. Djelloul, Appl. Phys. A 126 (2020) 122.
[26] S. Goel, N. Sinha, H. Yadav, A.J. Joseph, B. Kumar, Physica E Low Dimens. Syst. Nanostruct. 91 (2017) 72–81.
[27] X.L. Xu, Y. Chen, S.Y. Ma, W.Q. Li, Y.Z. Mao, Sens. Actuators B 213 (2015) 222–233.
[28] O. Lupan, T. Pauporte, L. Chow, B. Viana, F. Pelle, L.K. Ono, B.R. Cuenya, H. Heinrich, Appl. Surf. Sci. 256 (2010) 1895.
[29] S. Roguai, A. Djelloul, Solid State Commun. 334–335 (2021), 114362.
[30] A.R. Babar, S.S. Shinde, A.V. Moholkar, C.H. Bhosale, J.H. Kim, K.Y. Rajpure, J. Alloys Comp. 509 (2011) 3108.
[31] V. Kamlesh Chandekar, M. Shkir, A. Khan, B.M. Al-Shehri, M.S. Hamdy, S. AlFaify, M. Ahmed El-Toni, A. Aldalbahi, A.A. Ansari, H. Ghaithan, J,, Photochem. Photobiol. A. (395) (2020), 112465.
[32] C.-L. Hsu, H.-H. Li, T.-J. Hsueh, ACS Appl. Mater. Interfaces 5 (2013) 11142–11151.
[33] H. Morkoç, U. Ozgur, Materials and Device Technology, Wiley-VCH Verlag GmbH & Co, KGaA, Weinheim, 2009, pp. 1–76.
[34] S. Roguai, A. Djelloul, T. Corinne Nouveau, A.A. Souier, M.B. Dakhel, J. Alloys Comp. 599 (2014) 150–158.
[35] A. Ashour, M.A. Kaid, N.Z. El-Sayed, A.A. Ibrahim, Appl. Surf. Sci. 252 (2006) 7844–7848.
[36] S. Oktik, Prog. Cryst. Growth Charact. 17 (1988) 171–240.
[37] Y. Bouznit, Y. Beggah, F. Ynineb, Appl. Surf. Sci. 258 (2012) 2967–2971.
[38] F. Xiao, R. Chen, Y.Q. Shen, Z.L. Dong, H.H. Wang, Q.Y. Zhang, H. Sun, J. Phys. Chem. C 116 (2012) 13458–13462.
[39] K. Vanheusden, W.L. Warren, C.H. Seager, D.R. Tallant, J.A. Voigt, B.E. Gnade, J. Appl. Phys. 79 (1996) 7983–7990.
[40] G. Xiong, U. Pal, J.G. Serrano, J. Appl. Phys. 101 (2007), 024317.
[41] K. Vanheusden, C. Seager, Wt. Warren, D. Tallant, J. Voigt,, Appl. Phys. Lett. 68 (1996) 403–405.
[42] D. Chen, Z. Wang, T. Ren, H. Ding, W. Yao, R. Zong, Y. Zhu, J. Phys. Chem. C 118 (2014) 15300–15307.
[43] G. Du, F. Xu, Z. Yuan, G. Van Tendeloo, Appl. Phys. Lett. 88 (2006), 243101.
[44] J. Hu, X. Ma, Z. Xie, N. Wong, C. Lee, S. Lee, Chem. Phys. Lett. 344 (2001) 97–100.
[45] D.S. Bohole, C.J. Spira, J. Am. Chem. Soc. (131) (229) 4397.
[46] B. Choudhury, A. Choudhury, Mater. Chem. Phys. 131 (2012) 666.
[47] D.K.C. MacDonald, Thermoelectricity: an Introduction to the Principles, Wiley, New York, London, 1962.
[48] S. Roguai, A. Djelloul, Inorg. Chem. Commun. 138 (2022), 109308.
[49] A. Vora-ud, T. Seetawan, W. Somkhunthot, N. Pimpabute, T. Burinprakhon, Energy Proc. 61 (2014) 2355.
[50] J. Boy, M. Handwerg, R. Ahrling, R. Mitdank, G. Wagner, Z. Galazka, S.F. Fischer, APL Mater. 7 (2019), 022526.
[51] A. Zevalkink, D.M. Smiadak, J. Blackburn, A.J. Ferguson, M.L. Chabinyc, O. Delaire, J. Wang, K. Kovnir, J. Martin, L.T. Schelhas, T.D. Sparks, S.D. Kang, M. T. Dylla, G.J. Snyder, B.R. Ortiz, E.S. Tobere, Appl. Phys. Rev. 5 (2018), 021303.
[52] H. Kind, H. Yan, B. Messer, M. Law, P. Yang, Adv. Mater. 14 (2002) 158.
[53] C. Soci, A. Zhang, B. Xiang, S.A. Dayeh, D.P.R. Aplin, J. Park, X.Y. Bao, Y.-H. Lo, D. Wang, Nano Lett. 7 (2007) 1003.
[54] T.P. Chen, S.J. Young, S.J. Chang, C.H. Hsiao, C.S. Huang, J. Electrochem. Soc. 159 (2012) J153–J157.
[55] S.J. Young, L.W. Jib, S.J. Changa, Y.K. Su, J. Cryst. Growth 293 (2006) 43.
[56] T. Shen, J. Wang, Z. Xia, X. Dai, B. Li, Y. Feng, Sens. Actuator A Phys. 307 (2020), 111989.
[57] Y-L. Chu, Sh-J. Young, T-T. Chu, A. Khosla, K-Y. Chiang and L-W Ji, ECS J. Solid State Sci. Technol.(10) (2021) 127001.
[58] Y-L. Chu, Sh-J. Young, L-W. Ji, I-T. Tang and T-T. Chu, Sensors. (20) (2020) 3861.
[59] Sh-J. Chang, B-G. Duan, Ch-H. Hsiao, Sh-J. Young, B-Ch. Wang, T-H. Kao, K-Sh. Tsai, and S-L. Wu, IEEE Photon. Technol. Lett. (25) (2013) 2043–2046.
[60] Y. Zong, Z. Li, X. Wang, J. Ma, Y. Men, Ceram. Int. 40 (2014) 10375–10382.
[61] S. Kumar, P. Sahare, Mater. Res. Bull. 51 (2014) 217–223.
[62] G. Lente, Deterministic kinetics in chemistry and systems biology, Springer, New York, 2015, pp. 52–58.
[63] L. Song, S. Zhang, X. Wu, Q. Wei, Ind. Eng. Chem. Res. 51 (2012) 4922–4926.
[64] M. Samadi, M. Zirak, A. Naseri, E. Khorashadizade, A.Z. Moshfegh, Thin Solid Films 605 (2016) 2–19.
[65] G. Rothenberger, J. Moser, M. Graetzel, N. Serpone, D.K. Sharma, J. Am. Chem. Soc. 107 (1985) 8054–8059.
[66] S.I. Shah, C. Huang, J. Chen, D. Doren, M. Barteau, Proceedings of the NSF Nanoscale Science and Engineering Grantees Conference, Arlington, VA, USA, 2003, pp. 16–18.
[67] G. Cappelletti, C. Bianchi, S. Ardizzone, Appl Catal B 78 (2008) 193–201.
[68] S. Suwanboon, P. Amornpitoksuk, A. Sukolrat, N. Muensit, Ceram. Int. 39 (2013) 2811–2819.
[69] R. Bomila, S. Srinivasan, S. Gunasekaran, A. Manikandan, J. Supercond. Nov. Magn. 31 (2018) 855–864.
[70] N. Kaneva, A. Bojinova, K. Papazova, J. Phys. Conf. Ser. 682 (2016), 012022.
[71] S. Anandan, A. Vinu, K.S. Lovely, N. Gokulakrishnan, P. Srinivasu, T. Mori, K. Ariga, J. Mol. Catal. A Chem. 266 (2007) 149–157.
[72] L. Xu, Y.-L. Hu, C. Pelligra, C.-H. Chen, L. Jin, H. Huang, S. Sithambaram, M. Aindow, R. Joesten, S.L. Suib, Chem. Mater. 21 (2009) 2875–2885.